Hindawi
Advances in Civil Engineering
Volume 2022, Article ID 9246692, 11 pages
https://doi.org/10.1155/2022/9246692

Research Article

Mechanical Behavior of Reactive Powder Concrete Subjected to Biaxial Loading

Ziruo Yu,[1] **Zhiguang Li**,[2] **Yuran Jiang**,[1] **and Yue Wang**[1]

[1]*School of Civil Engineering, Beijing Jiaotong University, Beijing 100044, China*
[2]*BCEG Advanced Construction Materials Technology Inc, Beijing 102600, China*

Correspondence should be addressed to Ziruo Yu; zryu@bjtu.edu.cn

Received 24 March 2022; Revised 22 May 2022; Accepted 25 May 2022; Published 1 July 2022

Academic Editor: Shiming Wang

To investigate the biaxial mechanical characteristics of reactive powder concrete (RPC), RPC plate specimens and bone-shaped specimens were tested under compression-compression and compression-tension loadings, respectively. The strengths and strains of the specimens were recorded, and the crack patterns and failure modes in various stress states were examined. Based on the test data, the characteristics of biaxial strength were analyzed, and a biaxial failure criterion was established. The characteristics of major stress-strain curves and failure modes in different biaxial stress states were determined. The results show that the ratio between the biaxial compression strength and the uniaxial compression strength was 1.44–1.58 for RPC. When the stress ratio under compression-tension was −0.05, the tensile strength decreased by 48%. Under compression-compression, the proportional limit of RPC was about 95%, and its peak strain was high. Under compression-tension, as the compressive stress increased, the elastic modulus decreased, and the peak strain in the tensile direction increased. When the RPC specimens were under compression-compression, the failure mode of RPC was splitting failure. Under compression-tension, the failure mode changed from single-crack tensile failure to multicrack compressive failure with increasing confining stress.

1. Introduction

Reactive powder concrete (RPC) is a new type of cementitious composite material with a low water-to-cement ratio (W/C) that consists of fine granular materials with optimized grading curves, reactive powder such as silica fume, and discontinuous internal fiber reinforcement [1, 2]. The material owes its ultrahigh performance to the densified, macrodefect-free concrete matrix and the small-sized steel fibers, which bridge the concrete matrix when cracks appear. RPC displays not only high strength (it can attend a cubic compressive strength of at least 100 MPa and uniaxial tensile strength of over 5 MPa) but also impressive durability [3–5]. Among the new generation of sustainable high-performance construction materials, RPC is appropriate for use to improve structural durability and enhance structural performance under extreme loading.

Concrete is inevitably in a biaxial stress state in many engineering structures. It has been shown that the compressive strength is higher than that of uniaxially tested concrete in the compression-compression (C-C) stress state [6–8], which suggests that the structural design of concrete under C-C may be too conservative if the design parameters are determined from uniaxial tests. Meanwhile, reduced tensile resistance is usually measured in the biaxial compression-tension (C-T) stress state [9–11]. If the strength of the complex stress state under C-T is not taken into consideration, the structure will crack and be prematurely destroyed during use. On the other hand, RPC differs from traditional concrete in several aspects, and the use of RPC in structural design may not be appropriate if the design parameters are determined from tests for traditional concrete. Therefore, it is important to gain a thorough understanding of the behavior of RPC under biaxial stress.

In terms of the biaxial performance of RPC, Ple et al. [12] conducted numerical and experimental tests on RPC reinforced by short steel fibers under biaxial tensile loading, measured the displacement field and the microstructural

stress concentration of RPC specimens, and investigated the mechanism involved in the RPC damage process. Yoo et al. [13] conducted a biaxial flexural behavior test on RPC using round panels and studied the toughness, cracking behavior, and load versus deflection response of RPC plate, and the study mainly focuses on the biaxial bending of RPC thin plate. Generally, limited literature is available on the biaxial performance of RPC, especially the biaxial C-C and C-T performance. Existing research on the mechanical properties of RPC under complex stress state mainly focuses on the triaxial response of RPC [14–16]. Therefore, further investigation is required to better understand and quantify the biaxial response of RPC.

In the study reported here, a series of specimens were tested to provide the necessary experimental data for the characterization of the biaxial response of RPC. The stress-strain curves, ultimate strengths, failure envelopes, and failure modes of RPC specimens subjected to biaxial loading were examined. The results of this investigation will provide the material parameters that are essential to the structural analysis of RPC structures.

2. Materials and Methods

In this research, RPC specimens were subjected to two types of biaxial loading, namely C-C and C-T, to identify the mechanical characteristics of RPC under biaxial stress.

2.1. Materials. Type I Portland cement, quartz sand, silica fume, steel fiber, superplasticizer, and water were used to cast the specimens of RPC. The 28 d compressive strength of cement was 55 MPa, and the flexural strength was 9 MPa. The quartz sand consisted of particles measuring 0.16–0.315 mm (fine quartz sand), 0.315–0.625 mm (medium quartz sand), and 0.625–1.25 mm (coarse quartz sand) combined in a mixing ratio of 2 : 4 : 1. The apparent densities of the fine, medium, and coarse sand were 2.634, 2.627, and 2.586 g·cm^{-3}, respectively, and the bulk densities were 1.440, 1.306, and 1.428 g·cm^{-3}, respectively. The fine steel fibers measured 13 mm in length and 0.22 mm in diameter, and the volume fraction of the steel fibers was 2.0%; the tensile strength of a steel fiber was 2800 MPa. The silica fume was a grayish-white powder with a density of 2.214 g·cm^{-3}, an average particle size of about 0.31 μm, and a specific surface area of 143100 cm^2·g^{-1}. The content of SiO_2 in the silica fume was >90 wt%. The water-reducing rate of the superplasticizer was 29%, and the solid content was 31%. The mixing proportion of the RPC specimens is shown in Table 1; the water/binder ratio for the RPC mixture was 0.14.

2.2. Specimens and Casting. 15 specimens each were cast for biaxial C-C and C-T tests. The dimensions of the biaxial test specimens are described in "*Geometry and Dimensions of Specimens*." Furthermore, three 100 × 100 × 100 mm cubes were cast to measure the cube compressive strength, and three 100 × 100 × 300 mm prisms were cast to measure the prism compressive strength and elastic modulus of the specimens.

To cast the specimens, according to the national standard of the People's Republic of China for reactive powder concrete (GB/T 31387-2015), sand and steel fibers were mixed together in the mixing machine for 3 min. Cement and silica fume were then added and mixed for 1 min. After the dry components were fully mixed, water and the superplasticizer were added and mixed for 5–8 min. Once the mixing process was completed, the batch of fresh concrete was tested. The slump of the RPC mixture was 120 mm. Specimens of the RPC were prepared by casting the mixture into molds. After casting, the specimens were kept in their molds for 36 h. They were then removed from the molds and placed in a curing box for curing. The curing temperature was set to 45°C for 2 h and then was raised to 60°C for 2 h. Finally, the temperature was increased to 75°C, and the specimens were removed from the curing box after 68 h. All specimens were cast and cured in the same manner.

2.3. Basic Mechanical Properties. The basic mechanical properties of the hardened concrete were measured according to GB/T 31387-2015. Using a universal testing machine with a maximum capacity of 3000 kN, cube compressive strength f_{cu}, prism compressive strength f_{cp}, and elastic modulus E of RPC were measured. The age of the specimens at testing was 56 days. The mechanical properties of RPC are listed in Table 2.

2.4. Test Setup. The tests were carried out with an Instron 8506 testing machine, as shown in Figure 1, with a loading capacity of 2000 kN in the vertical direction and 1000 kN in the horizontal direction. The test setup consisted of three independent actuators, each of which was attached to a surface of the specimen with a steel plate. The closed-loop setup was controlled by the Instron 8506 Console software.

Owing to the friction between the specimen surfaces and the steel plates of the testing machine, the concrete specimen in a compressive state may be restrained along its loaded surfaces. To minimize this restraint in this test, Teflon sliding pads were placed between the loading plates and the specimen surfaces that were subjected to compression loads. The thickness of each Teflon pad used in this test was 0.2 mm.

2.5. Geometry and Dimensions of Specimens. RPC plates with dimensions of 150 × 150 × 50 mm (Figure 2(a)) were selected as specimens for the biaxial C-C tests, and both the vertical actuator and the horizontal actuator applied compressive force on the specimens.

For the C-T tests, 150 × 150 × 50 mm plates could also be used, but some issues must be taken into account: during the test, the horizontal actuator applies compressive force, and the vertical actuator applies tensile force on the specimen, which is directly glued to the tensile loading plates. In order to enable successful testing, the epoxy's bond strength should be carefully considered to ensure that it would securely hold the specimen in the direction of the applied tensile force. Most of the existing research [1, 3–5] showed that the uniaxial tensile strength of an RPC specimen was approximately 5–11 MPa,

Table 1: Mixing proportion of raw materials.

Cement (kg·m^{-3})	Quartz sand (kg·m^{-3})	Silica fume (kg·m^{-3})	Steel fiber (kg·m^{-3})	Superplasticizer (kg·m^{-3})	Water (kg·m^{-3})
706	1249	160	160	74	122

Table 2: Basic mechanical properties of specimens.

Mechanical properties	Specimen size (mm)	Mean value (MPa)	Standard deviation (MPa)	Coefficient of variation
Cube compressive strength, f_{cu}	$100\times100\times100$	102.8	4.32	0.042
Prism compressive strength, f_{cp}	$100\times100\times300$	83.7	3.26	0.039
Elastic modulus, E	$100\times100\times300$	3.82×10^4	0.21×10^4	0.055

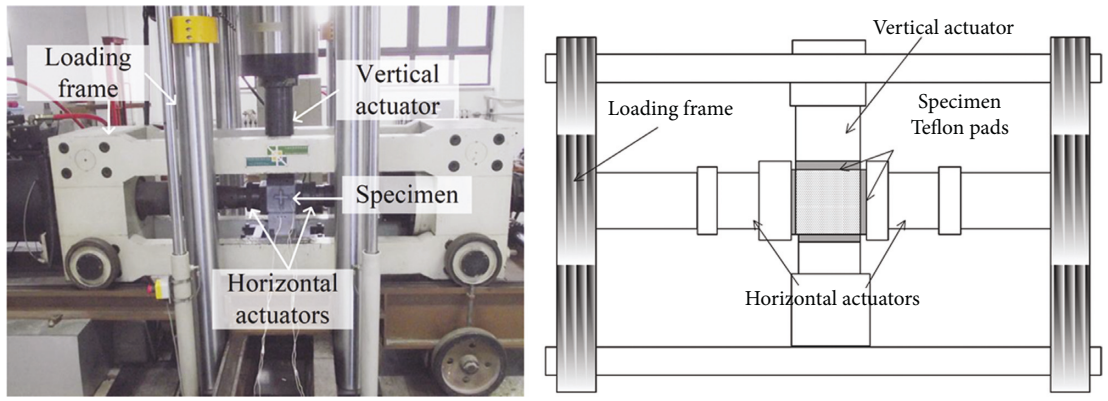

Figure 1: Biaxial test setup of RPC specimens.

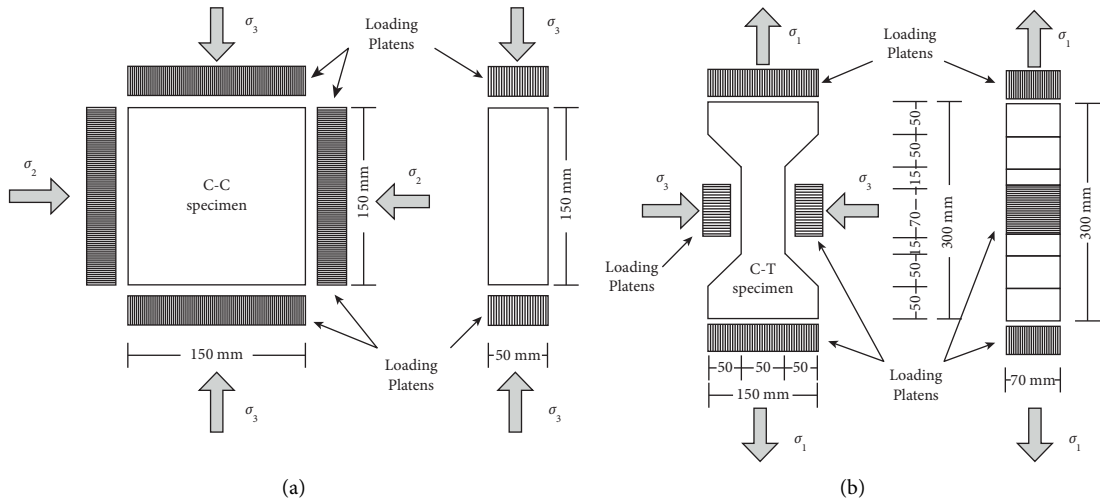

Figure 2: Geometric dimensions of RPC specimens used in the (a) C-C and (b) C-T tests.

while the tensile strength of the epoxy was 3-4 MPa. If a $150\times150\times50$ mm plate is used, the tensile boundary area is the same as the testing area of the specimen, and the epoxy at the edges would not provide a sufficient overall bonded tensile force for destructive tensile testing. Therefore, bone-shaped specimens were selected. Suitable dimensions were calculated for the specimens, and the area of the end of the specimen, which was used for bonding, was three times the area of the middle of the specimen, which was used for testing. Figure 2(b) shows the shape and dimensions of the C-T specimens used in this study.

2.6. Loading Method. In this research, the values of stress, σ, and strain, ε, along the three axes decreased in the order $\sigma_1 \geq \sigma_2 \geq \sigma_3$ and $\varepsilon_1 \geq \varepsilon_2 \geq \varepsilon_3$. When σ_i and ε_i were positive, the specimen was in tension; when σ_i and ε_i were negative, the specimen was in compression.

The method of displacement control was used for the tests. For the C-C ($\sigma_3 \leq \sigma_2 < 0$, $\sigma_1 = 0$) tests (Figure 2(a)), a loading scheme with proportional displacement was used; that is, the load was applied as the nominal strain ratios k ($k = \varepsilon_2/\varepsilon_3$) in the two directions. Four different biaxial nominal strain ratios ($k = 0.4$, 0.6, 0.8, and 1.0) were chosen, and three specimens were

Table 3: Strength of RPC specimens under compression-compression.

Nominal strain ratio, $k = \varepsilon_2/\varepsilon_3$	Specimen	Stress ratio, $\alpha = \sigma_{2c}/\sigma_{3c}$	σ_{2c} (MPa)	σ_{3c} (MPa)	$\lvert\sigma_{2c}\rvert/f_c$	$\lvert\sigma_{3c}\rvert/f_c$	σ_{3c} (predicted) (MPa)
Uniaxial compression	1	0.00	0.00	−86.7	0.00	1.07	−81.0
	2	0.00	0.00	−74.7	0.00	0.92	−81.0
	3	0.00	0.00	−82.5	0.00	1.02	−81.0
	Average	0.00	0.00	−81.3	0.00	1.00	−81.0
	Standard deviation	—	—	6.1	—	—	—
	Coefficient of variation	—	—	−0.07	—	—	—
0.4	1	0.40	−50.9	−125.9	0.63	1.55	−120.4
	2	0.42	−54.1	−128.3	0.67	1.58	−120.8
	3	0.45	−44.1	−98.6	0.54	1.22	−119.0
	Average	0.42	−49.7	−117.6	0.61	1.45	−120.2
	Standard deviation	—	5.1	16.5	—	—	—
	Coefficient of variation	—	−0.10	−0.14	—	—	—
0.6	1	0.39	−46.9	−121.7	0.58	1.50	−119.6
	2	0.50	−54.8	−110.1	0.68	1.36	−120.9
	3	0.46	−55.3	−119.2	0.68	1.47	−121.0
	Average	0.45	−52.3	−117.0	0.65	1.44	−120.6
	Standard deviation	—	4.7	6.10	—	—	—
	Coefficient of variation	—	−0.09	−0.05	—	—	—
0.8	1	0.55	−82.3	−149.7	1.02	1.85	−121.4
	2	0.79	−107.1	−135.4	1.32	1.67	−118.3
	3	0.81	−80.8	−100.0	1.00	1.23	−121.5
	Average	0.72	−90.0	−128.4	1.11	1.58	−120.7
	Standard deviation	—	14.8	25.5	—	—	—
	Coefficient of variation	—	−0.16	−0.20	—	—	—
1.0	1	0.69	−82.9	−120.9	1.02	1.49	−121.4
	2	0.87	−97.5	−111.7	1.20	1.38	−119.8
	3	0.74	−92.2	−124.6	1.14	1.54	−120.5
	Average	0.76	−90.9	−119.1	1.12	1.47	−120.6
	Standard deviation	—	7.4	6.7	—	—	—
	Coefficient of variation	—	−0.08	−0.06	—	—	—

tested for each value of k. The loading rate in the direction of σ_3 was 0.03 mm·min^{-1}, and the loading rate in the direction of σ_2 was 0.012, 0.018, 0.024, and 0.03 mm·min^{-1} for $k = 0.4$, 0.6, 0.8, and 1.0, respectively. In addition, three uniaxial plate specimens were tested. That is, for the specimen shown in Figure 2(a), only the displacement was applied in the direction of σ_3, and the performance of the specimens when the direction of σ_2 is not restrained was measured for comparison.

For the C-T ($\sigma_3 \le \sigma_2 = 0 \le \sigma_1$) tests (Figure 2(b)), the compression stress was set at $|\sigma_3| = 0$, $0.2f_c$, $0.4f_c$, $0.6f_c$, and $0.8f_c$, where f_c is defined as the uniaxial compressive strength of RPC plate specimens. Three specimens were tested for each σ_3. Along the tensile axis, σ_1 was applied after the target confining pressure, σ_3, was reached. The loading rate in the direction of both σ_1 and σ_3 was 0.03 mm·min^{-1}. Specifically, when $\sigma_3 = 0$, the specimen is in a stress state of uniaxial tensile, and the σ_1 measured under this condition is the uniaxial tensile strength f_t of RPC.

2.7. Data Collection. The stresses σ_1 (or σ_2) and σ_3 were measured using two loading cells mounted on the bottoms of the actuators. Deformation of the specimens in the direction of the movement was measured using linear variable differential transformers (LVDTs) contained in the Instron loading cells.

However, the deformation measured by the LVDTs was a combination of the deformation of the specimen and the deformation of the Teflon sliding pads. To obtain the true strain of the RPC specimens, it was necessary to deduce the deformation of Teflon sliding pads from the deformation measured by the LVDTs. A steel specimen with the same dimensions as those of the RPC specimens was tested to obtain the stress-deformation relationship. Then, the stress-deformation relationship of the Teflon pads was calculated from the following equation:

$$\Delta(\sigma) = L\left[\epsilon_1(\sigma) - \epsilon_2(\sigma)\right], \tag{1}$$

where $\Delta(\sigma)$ is the deformation of the Teflon pads, $\epsilon_1(\sigma)$ is the global strain measured by the LVDTs, $\epsilon_2(\sigma)$ is the strain of the steel specimen measured by strain gauges, and L is the length of the steel specimen. The true deformation of the RPC specimens was then obtained by deducing the deformation of the Teflon pads from the deformation by the LVDTs.

3. Results and Discussion

3.1. Biaxial Strength of Specimens. Tables 3 and 4 list the ultimate strength of the RPC specimens under different biaxial loadings. The values of σ_{1c}, σ_{2c}, and σ_{3c} represent the ultimate strength in the direction of σ_1, σ_2, and σ_3, respectively. To compare the effect of lateral stress σ_2 on the biaxial mechanical properties of RPC specimens with the same shape and size, f_c is the uniaxial compressive strength of RPC plate specimens (see Figure 2(a)). Thus, in Table 3, f_c is equal to σ_{3c} under the uniaxial compression. It can be seen that the coefficients of variation of σ_{2c} and σ_{3c} under C-C loading varied between −0.05 and −0.20, and the coefficient of variation of σ_{1c} under C-T loading varied between 0.02 and 0.16. The dispersion of the test results varies from 2% to 20%.

Table 3 shows that for the RPC specimens under C-C loading, the confinement stress along the minor axis, σ_2, had an obvious effect on the ultimate compressive strength, σ_{3c}. Owing to the increase in σ_2, σ_{3c} increased. At a nominal strain ratio of 0.4 and 0.6, σ_{3c} of the RPC specimens increased by 44–45% above the uniaxial strength f_c. Compared with the case of uniaxial compression (Table 3), the lateral compressive stress σ_2 exerted a restraining effect. σ_2 limited the development of microcracks in the RPC, which prevented the accumulation of internal damage, thus increasing the C-C strength. At a nominal strain ratio of 0.8, σ_{3c} reached a maximum, and the increase in strength was 58%. When the nominal strain ratio was 1.0, the increase in strength decreased to 47%. In other words, in the biaxial C-C tests, the strength enhancement ratio ($|\sigma_{3c}|/f_c$) between the biaxial compressive strength σ_{3c} and the uniaxial compression strength f_c was 1.44–1.58 in RPC. The maximum increase in the biaxial strength of RPC occurred at a nominal strain ratio of 0.8, with a corresponding stress ratio ($\alpha = \sigma_{2c}/\sigma_{3c}$) of 0.72.

In contrast, the increase in biaxial strength was 1.16 [17], 1.28–1.33 [18], and 1.48 [6] for normal strength concrete (NSC), 1.11 [19] and 1.24–1.50 [20] for steel fiber reinforced concrete (SFRC), and 1.15 [21] and 1.31 [22] for high strength concrete (HSC). It means that the strength enhancement ratio of RPC was higher than that of traditional concrete. The strength enhancement of RPC beyond that of NSC and HSC is attributed to the presence of steel fibers, which provide an "equivalent confining pressure" that acts perpendicular to the plane of the applied stress [10], reduced out-of-plane expansion, and improved the relative increase in strength when compared to that in NSC and HSC. Furthermore, the fine steel fibers in RPC have an extremely strong restraining effect. This was illustrated in the single-fiber extraction test and scanning electron microscopy analysis of Ju et al. [23] on the mechanism of steel fiber reinforcement in RPC. This study showed that because of the friction between the debris on the rough failure section and the matrix, and the effect of steel fibers in the matrix of the failure section, the steel fibers need to overcome a large sliding resistance and consume a large amount of energy before slipping can occur. This makes the strength enhancement ratio of RPC higher than that of SFRC.

For the RPC specimens subjected to C-T loadings, it can be seen in Table 4 that the tensile strength under biaxial C-T loading, σ_{1c}, was lower than that under uniaxial tension ($f_t = 6.6$ MPa), which is the average measure of σ_{1c} for $\sigma_{3c} = 0$. σ_{1c} decreased as the horizontal stress σ_{3c} increased. Under biaxial C-T loading, the horizontal stress σ_3 produced additional tensile strain. $\mu\sigma_3/E$, in the σ_1 direction, where μ is Poisson's ratio and E is the modulus of elasticity. As a result, the C-T strength of RPC was reduced. In this study, when $|\sigma_{3c}|/f_c = 0.8$ (i.e., when $\alpha = \sigma_{1c}/\sigma_{3c} = -0.054$), the tensile strength decreased by 48% from 6.6 MPa under uniaxial stress to 3.4 MPa under C-T loading. According to biaxial C-T research reported in the literature, when $\alpha = \sigma_{1c}/\sigma_{3c} = -0.05$, the tensile strength decrease was 35% [24], 59% [25], and 65% [26] for NSC, SFRC, and HSC, respectively. This means that under C-T loading, the relative decrease in tensile strength was higher for RPC than NSC but lower than for SFRC and HSC. Normally, the brittleness of concrete is higher for higher values of concrete strength. This comparison indicates that owing to the addition of steel fibers in the RPC examined in this study, it was more ductile than HSC despite the high strength. Since the steel fibers in RPC need to consume a larger amount of energy before slipping can occur [23], RPC was more ductile than SFRC. Therefore, the strength decrease ratio of RPC was lower than that of SFRC.

3.2. Failure Criterion for RPC. Based on the test results, the relationship between the normalized stresses, σ_{1c}/f_c (or σ_{2c}/f_c) and σ_{3c}/f_c, under C-T and C-C loadings are shown in Figure 3. The test results for each of the three specimens are represented by small open circles, and the average of the results is represented by black dots.

Among the failure criteria proposed for concrete, the most widely used one was established by Kupfer and Gerstle [27]. This criterion is represented by the following equations:

$$\left(\frac{\sigma_3}{f_c} + \frac{\sigma_2}{f_c}\right)^2 + A \cdot \frac{\sigma_2}{f_c} + \frac{\sigma_3}{f_c} = 0, \text{for} \frac{\sigma_3}{f_c} \le \beta, \tag{2}$$

$$\frac{\sigma_1}{f_c} = \left(1 + B \cdot \frac{\sigma_3}{f_c}\right) \cdot \frac{f_t}{f_c} \text{for} \frac{\sigma_3}{f_c} \ge \beta, \tag{3}$$

where f_c and f_t are the uniaxial compression and tension strength, respectively, of concrete. These two equations depend on the parameters A, B, and β. According to Kupfer and Gerstle [27], $A = 3.65$, $B = 0.8$, and $\beta = -0.96$ for NSC. The strength envelope they obtained for NSC is also shown as a dashed line in Figure 3. As shown in Figure 3, for the RPC specimens, in the C-T region with lower lateral pressure ($|\sigma_{3c}| \le 0.8\ f_c$), the strength envelope can be expressed as a straight line, that is, equation (3). In the C-C region, the

Table 4: Strength of RPC specimens under compression-tension.

Applied compression, σ_{3c} (MPa)	Specimen	Stress ratio, $\alpha = \sigma_{1c}/\sigma_{3c}$	σ_{1c} (MPa)	$\lvert\sigma_{1c}\rvert/f_c$	$\lvert\sigma_{3c}\rvert/f_c$	σ_{1c} (predicted) (MPa)
0 (uniaxial tension)	1	∞	6.7	0.08		
	2	∞	6.5	0.08	0	6.6
	3	∞	6.6	0.08		
	Average	∞	6.6	0.08	0	6.6
	Standard deviation	—	0.1	—	—	—
	Coefficient of variation	—	0.02	—	—	—
−15.9	1	−0.34	5.3	0.07		
	2	−0.38	6.0	0.07	0.2	5.5
	3	−0.36	5.8	0.07		
	Average	−0.36	5.7	0.07	0.2	5.5
	Standard deviation	—	0.4	—	—	—
	Coefficient of variation	—	0.06	—	—	—
−31.9	1	−0.13	4.2	0.05		
	2[a]	−0.20	6.3	0.08	0.4	4.5
	3	−0.16	5.2	0.07		
	Average	−0.15	4.7	0.06	0.4	4.5
	Standard deviation	—	0.8	—	—	—
	Coefficient of variation	—	0.16	—	—	—
−47.9	1	−0.07	3.2	0.04		
	2	−0.07	3.5	0.04	0.6	3.4
	3	−0.08	3.9	0.05		
	Average	−0.07	3.5	0.04	0.6	3.4
	Standard deviation	—	0.3	—	—	—
	Coefficient of variation	—	0.09	—	—	—
−63.8	1	−0.06	3.7	0.05		
	2[a]	−0.08	5.4	0.07	0.8	2.4
	3	−0.05	3.2	0.04		
	Average	−0.06	3.4	0.04	0.8	2.4
	Standard deviation	—	0.3	—	—	—
	Coefficient of variation	—	0.10	—	—	—

Note. [a]Fracture and failure of these two specimens occurred in the transitional cross section of the specimens, rather than in the C-T loading region. The strength and strain of these two specimens were very different from the average values among other specimens. Therefore, these two data points were omitted.

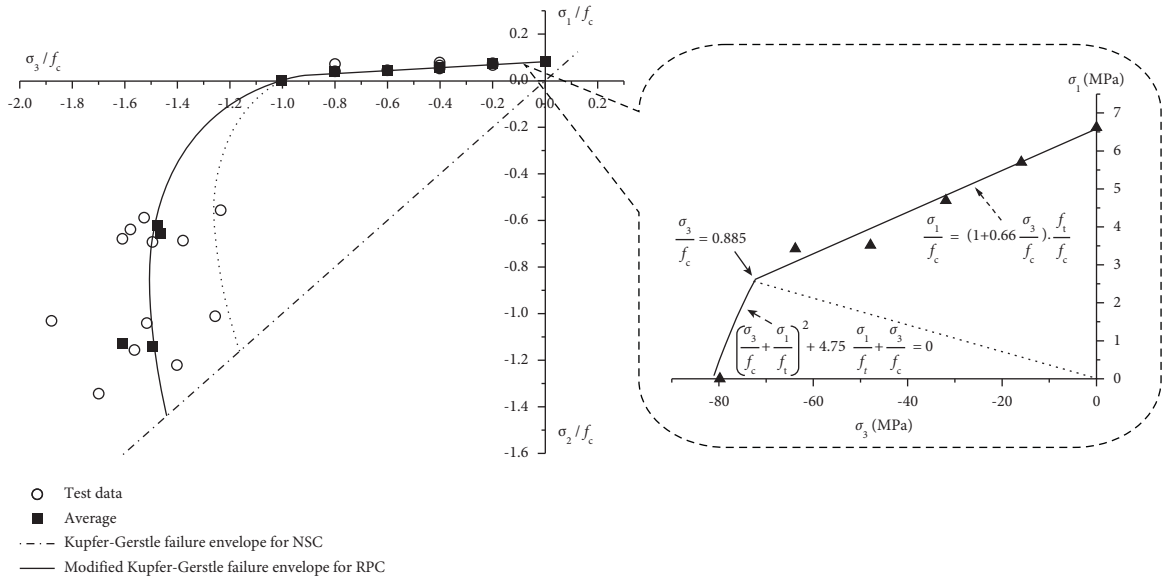

Figure 3: Failure envelope for RPC under biaxial stress.

relative increase in the biaxial C-C strength of RPC was larger than that of NSC. Because the fine, high-strength steel fibers in RPC exerted an excellent crack-resistance effect, the biaxial strength of the concrete was fully developed. Therefore, equation (2) could not be directly applied to RPC. However, since the trend of strength increase of RPC was the same as that of NSC, the biaxial strength envelope of RPC could be re-established by revising the parameters in the Kupfer–Gerstle failure criterion.

The way to revise the failure criterion was as follows. For the C-C region, the test data of RPC were used to fit the equation (2), and then, the parameter A suitable for RPC would be obtained. For the C-T region, on the side where the compressive stress is smaller ($|\sigma_{3c}| \le 0.8\, f_c$), the test data of RPC were used to fit the equation (3), followed by obtaining a suitable parameter B. On the side with the larger compressive stress ($|\sigma_{3c}| \ge 0.8\, f_c$) in the C-T region, equation (2) was still used. To ensure that the failure criterion is continuous in the C-T region, β, the position of turning point was obtained by requiring equations (2) and (3) to have equal stress states.

Through regression analysis, modified values of the parameters were obtained as $A = 4.75$, $B = 0.66$. The calculated $|\sigma_{3c}|$ at the turning point is 71.9 MPa, and the corresponding β is −0.885. Using these modified parameters, the biaxial failure criterion of RPC is given by

$$\left(\frac{\sigma_3}{f_c}+\frac{\sigma_2}{f_c}\right)^2 + 4.75\frac{\sigma_2}{f_c}+\frac{\sigma_3}{f_c} = 0, \quad \text{for} \quad \frac{\sigma_3}{f_c} \le -0.885,$$
$$\frac{\sigma_1}{f_c} = \left(1 + 0.66\frac{\sigma_3}{f_c}\right)\cdot\frac{f_t}{f_c}, \quad \text{for} \quad \frac{\sigma_3}{f_c} \ge -0.885. \tag{4}$$

The correlation coefficient, R, between the predicted values and the experimental results was about 0.98 and 0.95 for equations (2) and (3), respectively. The predicted values of σ_{3c} and σ_{1c} are listed in Tables 3 and 4, respectively. It can be seen that the modified failure criterion could give a good prediction of the strength of RPC under biaxial loading conditions.

3.3. Stress-Strain Relationships. Figure 4 shows the typical stress-strain curves of major axial loading (σ_3 for C-C, σ_1 for C-T) under various stress conditions. In Figure 4, the horizontal axis shows the strain and the vertical axis represents the stress of RPC specimens.

For the specimens under C-C loading (Figure 4(a)), the initial tangential inclination of their respective stress-strain curves is relatively steep for $k > 0$, but it is relatively gentle for uniaxial compression (i.e., $k = 0$). Under uniaxial compression, the elastic modulus in the σ_3 direction was E, and the elastic modulus in the σ_3 direction under C-C was $E/(1 - \alpha\mu) > E$, where α is the stress ratio of the biaxial compressive stress, and μ is Poisson's ratio. On the other hand, the horizontal pressure σ_2 prevented the development of microcracks and also increased the stiffness of the specimen. Therefore, the introduction of stress σ_2 significantly affected the stiffness of the RPC specimen in the direction of the major stress σ_3.

The proportional limit can be defined as the point at which the stress-strain curve deviates from linearity. Under uniaxial compression ($k = 0$), the stress-strain curves of the RPC specimens were almost linear up to 85% of the strength, which is higher than the proportional limits of 30–40% [28], 50–60% [29], and 60–70% [29] for NSC, SFRC, and HSC, respectively. This can be explained by the few initial defects in the RPC matrix, and the microcracks could remain stable for a long time. Moreover, the stress-strain curves for specimens under C-C loading were almost linear, with proportional limits of about 95%. The higher proportional limit was due to the introduction of stress σ_2, which prevented and delayed the creation of internal microcracks, resulting in a more linear stress-strain response. For RPC specimens under C-C loading, the strain corresponding to the peak stress ε_{3c} could reach 0.0025–0.0035, which is higher than the corresponding value of 0.0018–0.0030 for NSC [6, 18, 28], because a large amount of energy was required to pull out the steel fibers from the matrix in RPC, and the steel fibers were blocked by other fibers in the matrix they were pulled out. Therefore, the steel fibers could effectively prevent the development of cracks and make the material more ductile, thus greatly improving the deformation ability of the specimen.

The stress-strain curves for the RPC specimens subjected to C-T are shown in Figure 4(b). The stiffness in the σ_1 direction decreased with increasing $|\sigma_{3c}|$, the absolute value of the horizontal compression. This resulted from the higher increase in the tensile strain in the tensile direction because of the increase in the σ_3 direction; thus, the elastic modulus in the σ_1 direction decreased. Figure 4(b) also shows that the horizontal compression (σ_3) had a pronounced effect on the major peak strain of RPC (ε_{1c}). Under uniaxial tension, the peak strain was 0.000367. When the horizontal compression $|\sigma_{3c}|$ was $0.2f_c$, the peak strain was 0.000414, which corresponds to a relative increase of 13%. When $|\sigma_{3c}|$ was between $0.4f_c$ and $0.6f_c$, the peak strain increased drastically. The maximum peak strain of 0.000917 occurred at $|\sigma_{3c}|$ of $0.8f_c$, which corresponds to a relative increase of 147%. With respect to the deformations, the results show that the introduction of horizontal compression increased the tensile strain at failure, indicating that RPC could sustain a larger amount of indirect tensile strain rather than direct tensile strain owing to the Poisson effect.

As shown in Figure 4(b), the postpeak curves of the corresponding uniaxial and biaxial specimens are similar. Softening was observed after the peak, which corresponds to increased deformation at reduced resistance. However, with the increase in the horizontal compression ($|\sigma_{3c}|$), softening became less obvious and the stress-strain curves appear smoother, indicating that the tensile strain caused by the Poisson effect gradually increased in proportion to the entire tensile strain.

3.4. Failure Modes. Figure 5 shows the crack patterns and failure modes of RPC specimens under uniaxial compressive stress and uniaxial tensile stress. Under uniaxial compression, the main crack appeared, and it was inclined along the

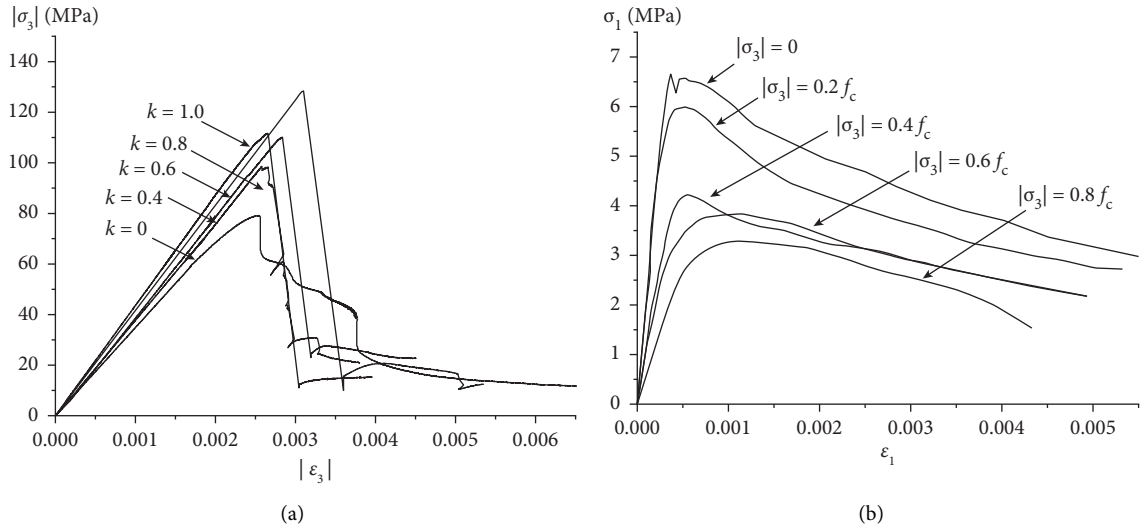

Figure 4: Stress-strain curves of RPC specimens under (a) C-C and (b) C-T.

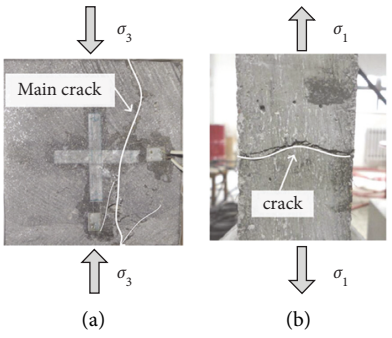

Figure 5: Failure modes of RPC under (a) uniaxial compression and (b) uniaxial tension loading.

loading direction; the crack pattern is highlighted by the white line in Figure 5(a). Owing to the effect of bridging by the steel fibers, the RPC specimens were still completely integrated after the tests. Under uniaxial tension, fracture and subsequent failure of the specimen occurred as a result of the formation of a single crack perpendicular to the direction of tensile loading, accompanied by significant pullout of the fibers (Figure 5(b)).

Figure 6 shows photographs of the crack patterns and failure modes of RPC specimens under C-C. Different types of cracks are represented by different line styles: main cracks are represented by solid lines, small cracks are represented by dashed lines, and minor cracks are represented by dash-dot lines.

In general, the failure mode of the RPC specimens under C-C loading was a splitting fracture in the plane of loading. At the nominal strain ratios of 0.4 and 0.6 (Figures 6(a) and 6(b)), the horizontal compressive stress σ_2 countered the expansion of the specimen along the σ_2 direction, so cracks on the top and bottom of the specimen appeared parallel or inclined to the loading plane. Failure of the specimens then occurred through the formation of a single crack that was inclined at an angle of 20° to 30° from the loading plane. When the nominal strain ratio was 0.8 (Figure 6(c)), several small oblique cracks developed on the free surface, while one major crack and one minor crack developed in the direction of the vertical load. The major crack was inclined to the direction of the loading plane. During the test, the concrete was partly spalled, which is consistent with the relatively larger strain of RPC specimens under C-C loading with $k = 0.8$. As the nominal strain ratio increased to 1.0, the multicrack splitting failure mode became very obvious, as shown in Figure 6(d).

Figure 7 shows the crack patterns and failure modes of RPC specimens subjected to C-T loading. Two different patterns of failure modes appeared.

Figures 7(a) and 7(b) show that for relatively smaller compressive stresses ($|\sigma_{3c}| = 0.2$–$0.4f_c$), the fracture of the specimen was determined by a major tensile crack inclined at an angle of about 10° from the direction of the applied compressive load. Some small tensile cracks perpendicular to the direction of the applied tensile load (σ_1) were also observed, but they were not fully developed. For larger compressive stress, the mode of crack propagation and development became close to those of uniaxial compression. Figure 7(c) shows that when $|\sigma_{3c}|$ was $0.6f_c$, even though

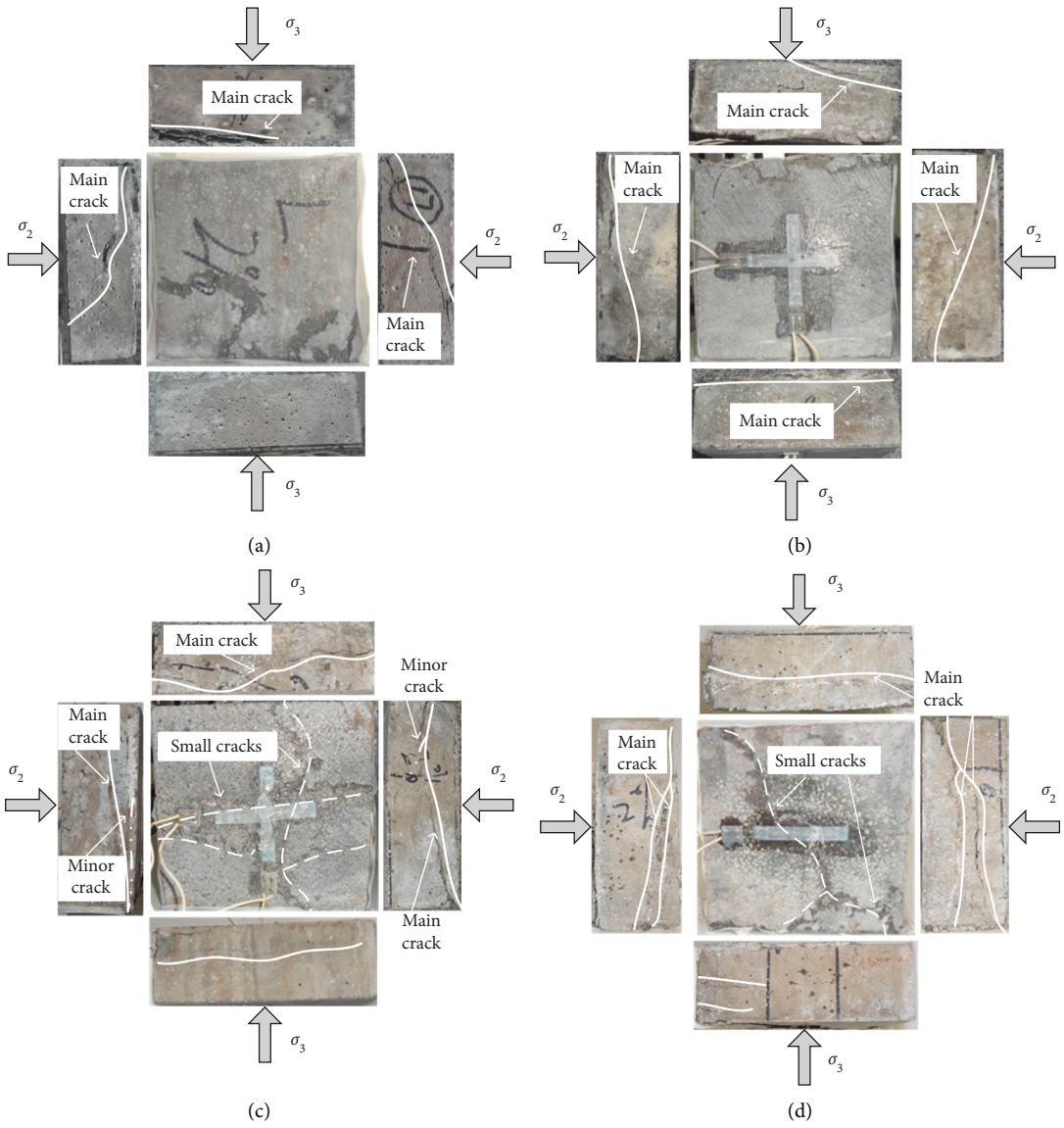

Figure 6: Failure modes of RPC C-C specimens under (a) $k = 0.4$, (b) $k = 0.6$, (c) $k = 0.8$, and (d) $k = 1$.

failure still occurred as a result of a single crack at the center of the specimen, several small tensile cracks parallel to the main crack developed. As $|\sigma_{3c}|$ increased to $0.8f_c$, another failure pattern was observed, as shown in Figure 7(d): the failure of the specimen was determined by several compressive cracks. All these cracks developed and merged until a wide crack developed at a 20–30° inclination from the direction of the compressive stresses. Therefore, it can be considered that the behavior in the zone of $|\sigma_{3c}| = 0.6f_c$ represented a transition from the behavior under uniaxial tension to that under uniaxial compression: for smaller compressive stresses ($|\sigma_{3c}| = 0.2$–$0.4f_c$), the crack shape and failure mode were similar to those of uniaxial tension, while for larger compressive stresses ($|\sigma_{3c}| = 0.8f_c$), more cracks developed, and the failure mode was similar to that of uniaxial compression. This phenomenon also responded to the failure criterion in the C-T region (Figure 3): when $|\sigma_{3c}|$ is relatively large, the failure criterion is shown in equation (2), indicating that the failure mode of the specimen was dominated by compressive failure; when $|\sigma_{3c}|$ is relatively small, the failure criterion is shown in formula (3), indicating that the failure mode of the specimens was dominated by tensile failure.

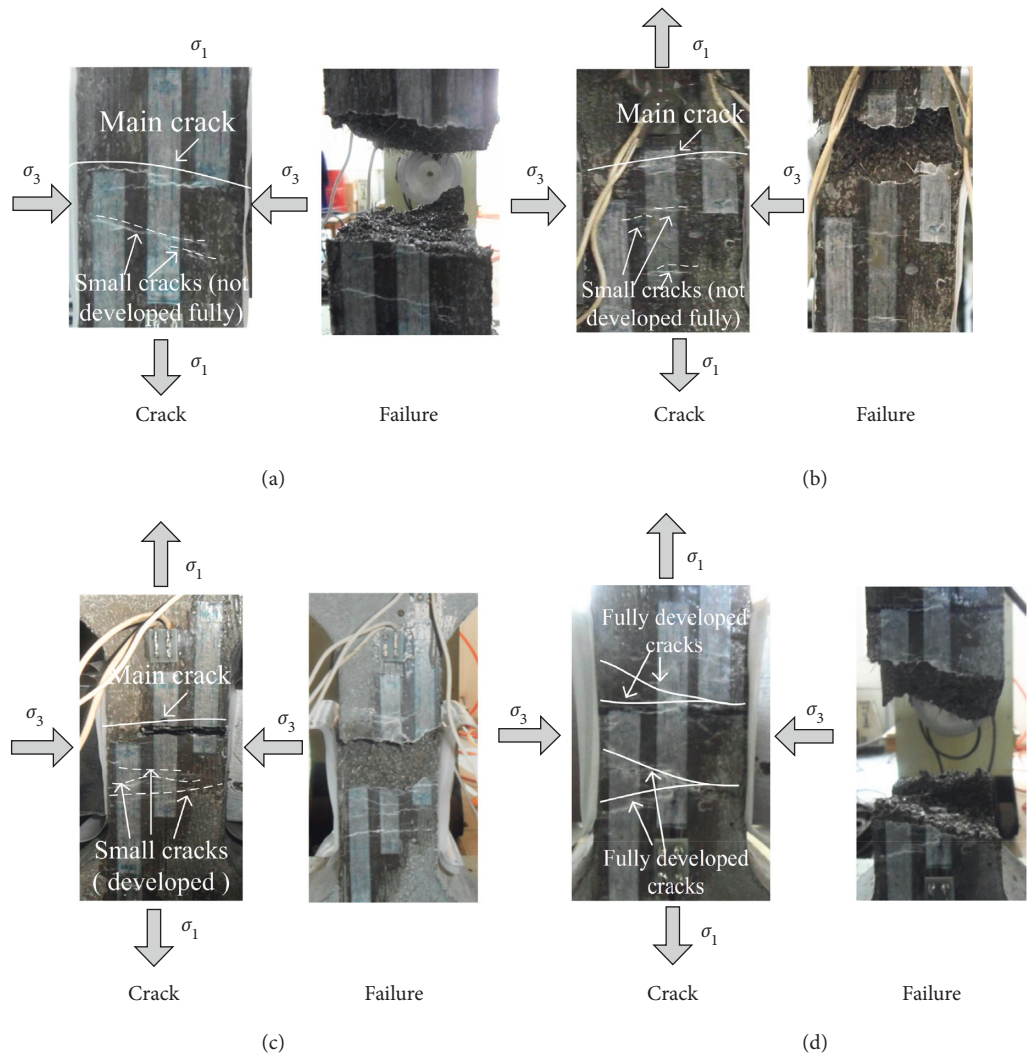

Figure 7: Failure modes of RPC C-T specimens under (a) $|\sigma_{3c}| = 0.2f_c$, (b) $|\sigma_{3c}| = 0.4f_c$, (c) $|\sigma_{3c}| = 0.6f_c$, and (d) $|\sigma_{3c}| = 0.8f_c$.

4. Conclusions

The behavior of RPC under biaxial stress states was experimentally investigated. Based on the test results, the following conclusions can be reached:

(1) The biaxial C-C strength of RPC was much higher than the uniaxial compressive strength. The ratio between the biaxial compression strength and the uniaxial compression strength was 1.44–1.58 in RPC. The maximum increase in the biaxial C-C strength of RPC was attained at a stress ratio of 0.72. The tensile strength of RPC under C-T loading decreased as the horizontal compressive stress increased. When the stress ratio was –0.05, the tensile strength decrease was 48%.

(2) The trend of biaxial strength envelope for RPC was the same as that described by the Kupfer–Gerstle relationship for NSC. Based on the test data, a modified failure criterion was suggested for RPC.

(3) Under C-C loading, as the horizontal compression increased, the stiffness of the RPC specimens increased. The peak strain of RPC was 0.0025–0.0035, which is higher than that of NSC. The proportional limit for the C-C RPC specimens was about 95%. Under C-T loading, the introduction of horizontal compression reduced the elastic modulus and increased the peak strain in the tensile direction. As the compressive stress increased, the stress-strain curves in the tensile direction became smoother.

(4) Under C-C loading, the failure mode of RPC was splitting failure. When the RPC specimens were under C-T loading, the failure mode changed from single-crack tensile failure to multicrack compressive failure with increasing confining stress.

Data Availability

The data used to support the findings of the study are available from the corresponding author upon request.

Conflicts of Interest

The authors declare that they have no conflicts of interest.

Acknowledgments

This work was supported by the Fundamental Research Funds for the Central Universities (Grant no. 2019JBM089) and the National Natural Science Foundation of China (Grant no. 52108189).

References

[1] P. Richard and M. Cheyrezy, "Composition of reactive powder concretes," *Cement and Concrete Research*, vol. 25, no. 7, pp. 1501–1511, 1995.

[2] S. Ahmed, Z. Al-Dawood, F. Abed, M. A. Mannan, and M. Al-Samarai, "Impact of using different materials, curing regimes, and mixing procedures on compressive strength of reactive powder concrete - a review," *Journal of Building Engineering*, vol. 44, Article ID 103238, 2021.

[3] M. Á. Sanjuán and C. Andrade, "Reactive powder concrete: durability and Applications," *Applied Sciences*, vol. 11, no. 12, p. 5629, 2021.

[4] Y. Wang, M.-z. An, Z.-r. Yu, S. Han, and W.-Y. Ji, "Durability of reactive powder concrete under chloride-salt freeze-thaw cycling," *Materials and Structures*, vol. 50, no. 1, p. 18, 2017.

[5] S. Doodala, V. Gayanipriya, and G. A. Chowdary, "Mechanical and durability properties of reactive powder concrete," *International Journal of Applied Research*, vol. 4, no. 1, pp. 31–35, 2018.

[6] H. Kupfer, H. K. Hilsdorf, and H. Rusch, "Behavior of concrete under biaxial stresses," *ACI J*, vol. 66, no. 8, pp. 656–666, 1969.

[7] X. Hu, R. Day, and P. Dux, "Biaxial failure model for fibre reinforced concrete," *Journal of Materials in Civil Engineering*, vol. 16, no. 5, pp. 609–615, 2003.

[8] J. Bao, L. Wang, Q. Zhang, Y. Liang, P. Jiang, and Y. Song, "Combined effects of steel fiber and strain rate on the biaxial compressive behavior of concrete," *Construction and Building Materials*, vol. 187, pp. 394–405, 2018.

[9] X. Ren, W. Yang, Y. Zhou, and J. Li, "Behavior of high-performance concrete under uniaxial and biaxial loading," *ACI Materials Journal*, vol. 105, no. 6, pp. 548–557, 2008.

[10] W. Swanepoel, "The Behaviour of fibre reinforced concrete (SHCC) under biaxial compression and tension," Master Degree Thesis, University of Stellenbosch, Stellenbosch, South Africa, 2011.

[11] H.-s. Shang, S.-t. Yang, and X.-Y. Niu, "Mechanical behavior of different types of concrete under multiaxial tension-compression," *Construction and Building Materials*, vol. 73, pp. 764–770, 2014.

[12] O. Ple, D. Astudillo, G. Bernier, and O. Bayard, "Biaxial tensile behavior of the reactive powder concrete," *Innovations in Design with Emphasis on Seismic, Wind, and Environmental Loading; Quality Control and Innovations in Materials/Hot-Weather Concreting. Cancun(MX)*, pp. 369–388, Ecole Normale Superieure de Cachan, Cachan, France, 2002.

[13] D.-Y. Yoo, G. Zi, S.-T. Kang, and Y.-S. Yoon, "Biaxial flexural behavior of ultra-highperformance fiber-reinforced concrete with different fiber lengths and placement methods," *Cement & Concrete Composites*, 2015.

[14] X. F. Wang and Y. P. Wang, "The conventional triaxial compressive test of plain reactive powder concrete," *Applied Mechanics and Materials*, vol. 670-671, pp. 401–406, 2014.

[15] Z. Yu, H. Zhao, M. An, and Y. Liu, "Mechanical properties of reactive powder concrete under triaxial compression," *Journel China Railway Society*, vol. 39, no. 7, pp. 117–122, 2017.

[16] Z. Wang and L. Wu, "Triaxial test study of reactive powder concrete with different sizes under different friction reducing conditions," *Journel Zhejiang University (Engineering Science)*, vol. 53, no. 1, pp. 40–50, 2019.

[17] M. E. Tasuji, F. O. Slate, and A. H. Nilson, "Stress-strain response and fracture of concrete in biaxial loading," *Journal of American Concrete Institute*, vol. 75, no. 7, pp. 306–312, 1978.

[18] S.-K. Lee, Y.-C. Song, and S.-H. Han, "Biaxial behavior of plain concrete of nuclear containment building," *Nuclear Engineering and Design*, vol. 227, no. 2, pp. 143–153, 2004.

[19] R. B. Abdull-ahad and J. M. Abbas, "Behaviour of steel fibre reinforced concrete under biaxial stresses," *Fibre Reinforced Cements and Concretes: Recent Developments*, pp. 18–20, University of Wales, Wales, UK, 1989.

[20] Y. L. Dong, C. M. Fan, and J. L. Pan, "Study on biaxial failure criteria of SFRC," *Journal of Harbin University of Civil Engineering and Institute*, vol. 26, no. 6, pp. 69–73, 1993.

[21] Y. T. Guo, *Experimental Study of Strength and Strain of High Strength concrete under Biaxial Stress*, Ph.D. thesis, Tsinghua University, Beijing, China, 1995.

[22] A. A. Hussein, *Behavior of High-Strength concrete under Biaxial Loading Conditions*, Ph.D. thesis, Memorial University of Newfoundland, St. John's, Newfoundland and Labrador, Canada, 1998.

[23] Y. Ju, Y. D. Jia, H. B. Liu, and J. Chen, "Microscopic mechanism of strengthening and toughening of reactive powder concrete steel fiber," *Science China Press*, vol. 37, no. 11, pp. 1403–1416, 2007.

[24] W. Z. Li and Z. H. Guo, "The strength and strain of concrete under biaxial compression-tension," *Journal of Hydraulic Engineering*, vol. 8, pp. 51–56, 1991.

[25] S. D. Zhang, Z. F. Shao, J. L. Pan, and C. M. Fan, "Behavior of plain concrete and SFRC under biaxial tension and biaxial tension-compression," *Journal of Harbin University of Architecture and Engineering*, vol. 30, no. 6, pp. 28–35, 1997.

[26] T. Hampel, K. Speck, S. Scheerer, R. Ritter, and M. Curbach, "High-performance concrete under biaxial and triaxial loads," *Journal of Engineering Mechanics*, vol. 135, no. 11, pp. 1274–1280, 2009.

[27] H. B. Kupfer and K. H. Gerstle, "Behavior of concrete under biaxial stresses," *Journal of the Engineering Mechanics Division*, vol. 99, no. 4, pp. 853–866, 1973.

[28] Z. H. Guo, *Strength and Deformation of concrete*, Tsinghua University Press, Beijing, China, 1997.

[29] Y. P. Song, *Constitutive Relationship and Failure Criterion for Different concrete Materials*, China Water & Power Press, Beijing, China, 2002.